Surface & Coatings Technology 203 (2009) 3676–3685

Contents lists available at ScienceDirect

Surface & Coatings Technology

journal homepage: www.elsevier.com/locate/surfcoat

Ion energy and mass distributions of the plasma during modulated pulse power magnetron sputtering

J. Lin [a], J.J. Moore [a,*], W.D. Sproul [a,b,*], B. Mishra [a], J.A. Rees [c], Z. Wu [a], R. Chistyakov [d], B. Abraham [d]

[a] Advanced Coatings and Surface Engineering Laboratory (ACSEL), Colorado School of Mines, Golden, Colorado, 80401 USA
[b] Reactive Sputtering, INC, 2152 Goya Place, San Marcos, California, USA
[c] Hiden Analytical Ltd, Warrington, England
[d] Zpulser, LLC, MA, USA

ARTICLE INFO

Article history:
Received 6 March 2009
Accepted in revised form 30 May 2009
Available online 10 June 2009

Keywords:
Modulated pulse power (MPP)
High power pulsed magnetron sputtering (HPPMS)
Ion energy distribution
Ion mass distribution
Plasma diagnostics
Ion flux

ABSTRACT

Modulated pulse power (MPP) sputtering is a variation of high power pulsed magnetron sputtering (HPPMS) that overcomes the rate loss issue and achieves enhanced plasma ionization through modulation of the pulse shape, intensity, and duration. In this study, the principle and characteristics of MPP/HPPMS technique are first introduced. An electrostatic quadrupole plasma mass spectrometer installed parallel to the target surface has been used to examine the plasma properties, including time averaged ion energy and mass distributions of the positive ions, generated during sputtering a metal Cr target in pure Ar and Ar/N_2 atmospheres using MPP and continuous dc power sources in a closed field unbalanced magnetron sputtering system. It was found that the MPP plasma exhibits a low ion energy peak at 1–2 eV and a short ion energy tail with the maximum ion energy affected by the peak current and power utilized on the cathode. A significantly increased numbers of single and double charged Cr and Ar ions were identified in the MPP plasma as compared to the dc plasma in pure Ar. The number of ions (ion flux) increased when the peak target power and current were increased. Besides single and double charged Cr, Ar and N ions, N_3^+, N_4^+, CrN^+ and CrN_2^+ ion species were also identified in the MPP discharge with the introduction of N_2 into the system. The ion energy distributions of ion species for the MPP plasma in Ar/N_2 atmosphere exhibit similar peak values and tail distributions to those of the MPP plasma in pure Ar atmosphere. However, the energy tail extended toward higher energies due to the increased peak current and power on the cathode as the N_2 flow rate percentage was increased in the system.

Published by Elsevier B.V.

1. Introduction

The new high-power pulsed magnetron sputtering (HPPMS) technique has been recently developed for sputter deposition and has attracted wide attention. It is also known as high-power impulse magnetron sputtering (HIPIMS). The HPPMS technique originally developed by Kouznetsov [1], is aimed at generating a high degree of ionization of the sputtered species to achieve high plasma density through using pulsed, high peak target power density for a short period of time [2–4].

In normal dc and pulsed dc magnetron sputtering, the degree of ionization of the sputtered material is low (typically less than 10%), which is due to the relatively low power density (e.g. 3–10 W cm^{-2}) used on the target to prevent the target overheating from ion bombardment [5,6]. However, in HPPMS, the average thermal load on the target is kept low by operating the target with a high peak power density (e.g. 1–3 kW cm^{-2}) for a short period of time (100–150 μs) and a low duty cycle (1–10%). Consequently a considerably larger fraction of ionized species can be created by the high probability for ionizing collisions between the sputtered atoms and energetic species. Extensive investigations have been carried out to study the HPPMS/HIPIMS plasma properties for different target materials using mass spectrometers and Langmuir probes in recent years [7–17]. It was found that the degree of ionization is strongly affected by the peak pulse power and the target material; e.g. it was reported that the fraction of ionized target species in HPPMS can be increased up to 70% or higher for Ti [18]. Significant improvements in coating structure and properties [19–25], uniform deposition [26,27], arc suppression [28], and enhanced coating adhesion [29,30,31] using HPPMS/HIPIMS have been reported. However, it was found that the deposition rate in HPPMS is lower than the dc rate for an equivalent amount of power [32]. The decreased deposition rate in HPPMS has been explained mainly in that the ions can be attracted back toward the target and captured by the negative potential on the cathode as proposed in the model developed by Christie [33].

In recent years, an alternative HPPMS deposition technique known as Modulated Pulse Power (MPP) has been developed that overcomes the rate loss problem while still achieving a high degree of ionization

* Corresponding authors. Tel.: +1 303 273 3771; fax: +1 303 273 3795.
E-mail addresses: jjmoore@mines.edu (J.J. Moore), bsproul@cox.net (W.D. Sproul).

0257-8972/$ – see front matter. Published by Elsevier B.V.
doi:10.1016/j.surfcoat.2009.05.048

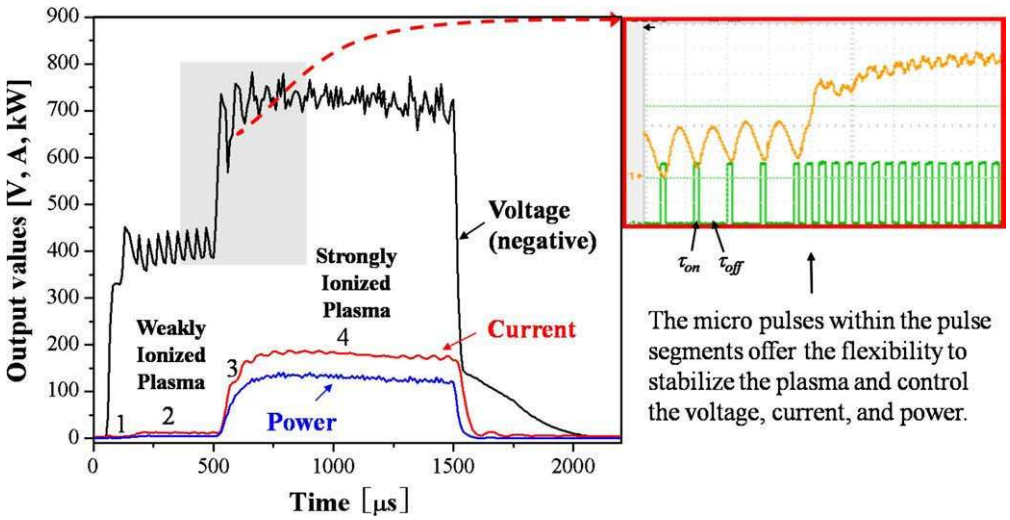

Fig. 1. Typical MPP pulse showing four steps of the target voltage, current and power evolutions during one modulated pulse (1500 μs overall pulse length in this example): 1) ignition of the weakly ionized plasma; 2) duration of the weakly ionized plasma; 3) transition stage from the weakly ionized plasma to the strongly ionized plasma; (4) duration of the strongly ionized plasma. The inserted figure on the right side shows the micro pulses within the pulse with adjustable voltage on (τ_{on}) and off (τ_{off}) times.

of the sputtered material [34–38]. The difference between the HPPMS and MPP techniques is that the pulse length with the MPP technique is in the 2–3 ms range, and there are multiple steps and micro pulses within one overall pulse period. Fig. 1 shows the target power, voltage, and current waveforms during one typical MPP pulse period (please note that the voltage values are negative). Unlike the simple one pulse shape in HPPMS as reported by Kouznetsov [1], MPP generates a high density plasma by first producing a weakly ionized plasma followed by a transition to a strongly ionized plasma within one overall pulse. The weak ionization pulse segment is used to ignite an initial stable discharge with low power and current (steps 1 and 2 in Fig. 1). Then a strong ionization pulse segment is generated with high power and current on the target as the main ionization stage (steps 3 and 4 in Fig. 1). The utilization of the transition step from weakly ionized to strongly ionized plasma is critical in obtaining stable discharges for different target materials in that it can make the generation of the high power pulse discharge much easier as compared to the situation when the high voltage and current are suddenly applied to the target.

In MPP, the maximum pulse width can be in the range of 500–3000 μs and the maximum duty cycle is 28%. The pulse frequency can be selected to be between 4 and 400 Hz. The MPP plasma generator is a switching power supply [39,40] which can control the voltage 'on' time (τ_{on}) (the width of micro pulses) and the voltage 'off' time (τ_{off}) (the distance between micro pulses) in the micro pulses (see the small insert graph on the right side in Fig. 1). By manipulating the pulse width, the frequency, and τ_{on} and τ_{off} in the micro pulses, MPP can generate a pulsed plasma with controllable peak power up to 360 kW, a maximum average power of 20 kW, and a maximum peak current of 550 A on the target during the strongly ionizing segment. In addition, given the flexibility to create multiple pulse steps within one pulse and to adjust the power and current in each step, together with an arc suppression capability, stable deposition processes can be achieved for sputtering various film materials and for reactive sputter deposition of oxides and nitrides.

The development of the MPP technique opens new approaches in the engineering and design of film materials with high deposition rates and improved microstructure and properties [34,35,36] by using the highly ionized and high density plasma. However, since the MPP/HPPMS technique is still in its early development stage, there is a need to understand the correlation between the high power pulse parameters and the plasma properties and to explore the potential for controlling the ion energy and ion flux in this new high power, pulsed plasma process to tailor the structure, adhesion, and properties of the films.

In the present investigation, we report results for the examination of the positive ion mass distributions (IMD), ion energy distributions (IED) and ion flux during sputtering of a metal Cr target in Ar and Ar/N_2 atmospheres using the MPP power source in a closed magnetic field unbalanced magnetron sputtering (CFUBMS) system. The plasma properties of a continuous dc discharge plasma generated at similar average target powers in the same deposition system were also investigated for comparison.

2. Experimental details

Fig. 2 shows the schematic drawing of the setup of the deposition system and the Electrostatic QuadruPole Plasma Mass Spectrometer (EQP) 300 (Hiden Analytical Ltd.). The deposition system is a cylindrical chamber (640 mm in diameter and 940 mm in height) that contains two unbalanced magnetrons of reversed magnetic polarities installed vertically to form a closed magnetic field. One Cr target with the dimension of 300 mm × 100 mm × 6.4 mm and 99.95% purity was

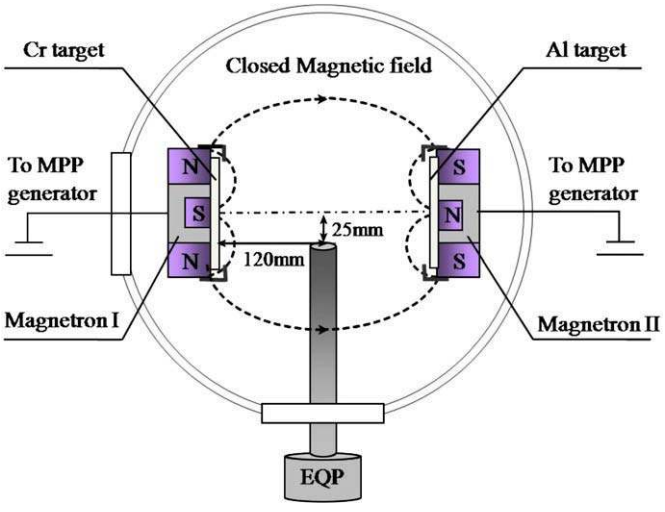

Fig. 2. Schematic drawing showing the setup of the CFUBMS system and the EQP probe from top view.

powered by a MPP generator (SOLO/AXIS-xxx™ AWF™ Pulsed DC Plasma Generator) manufactured by Zpulser, LLC and a dc power supply (Pinnacle) manufactured by Advanced Energy Inc. The other target was not powered in the current study but was used to close the magnetic field. The effective sputter area within the sputter track was estimated to be 180 mm^2, which was used to calculate the current densities on the target. The distance between the two targets is about 240 mm.

In the current study, the total pulse width in MPP was fixed at 750 μs, which consists of a 500 μs weakly ionized period and a 250 μs strongly ionized period. The pulse frequency was fixed at 100 Hz. The τ_{off} and τ_{on} in the micro pulses during the weakly ionized period were set at 34 and 6 μs respectively, and these conditions generated a low peak power of 4.5 kW and a peak current of 12 A on the target. However, the τ_{off} for the micro pulse during the strongly ionized period was set at 6 μs, while the τ_{on} was varied from 6 to 16 μs to generate different peak powers, voltages, and currents on the target during the strongly ionized period. For the continuous dc sputtering, the target power was regulated from 0.5 W to 4 kW.

Ar and N_2 gas flows were introduced into the system through feedthroughs in the side of the chamber and regulated by the MKS 146C vacuum gauge measurement system together with separate MKS 100 sccm mass flow controllers. During plasma diagnostics, the total gas flow rate was maintained constantly at 55 ± 1 sccm and balanced with a controlled pumping speed to achieve a constant working pressure of 0.67 Pa in the chamber.

The EQP uses an electrostatic sector field energy analyzer for ion energy analysis. The energy analyzer is followed by a triple section quadrupole mass filter. The EQP can be operated in two modes: (i) the PI (plasma ions) mode, in which the ions are directly extracted from the plasma and focused into the energy filter; and (ii) the EI (electron impact) mode, in which neutrals and radicals are sampled from the plasma and ionized inside an EI ion source to be focused into the energy filter. Both the ions formed in the plasma (in the PI mode) and the internally generated ions (in the EI mode) represent the instantaneous status of the plasma during film depositions.

In this study, an ion energy distribution (IED) was obtained by varying the potential in the energy analyzer and fixing the mass filter to allow only ions with a certain mass to charge ratio to reach the detector. The ion mass distribution (IMD) was obtained by fixing the energy filter to allow only ions with a given energy in a small energy range to reach the mass detector. The EQP probe was installed parallel to the target surface through the side of the chamber (Fig. 2). The EQP axis was placed exactly along the middle line between two targets. The distance between the target surfaces to the EQP probe was 120 mm. The diameter of the orifice in the front of the EQP is 100 μm, the orifice being about 25 mm away from the center of the chamber, as shown in Fig. 2.

The time-averaged IEDs of $^{52}Cr^+$, $^{52}Cr^{2+}$, $^{40}Ar^+$, $^{28}N_2^+$ and $^{14}N^+$, for various discharge parameters were examined in the PI mode (in the expression $^mA^e$, A is the ion species, m is the mass, and e is the charge). The EQP probe was tuned for each species to achieve the

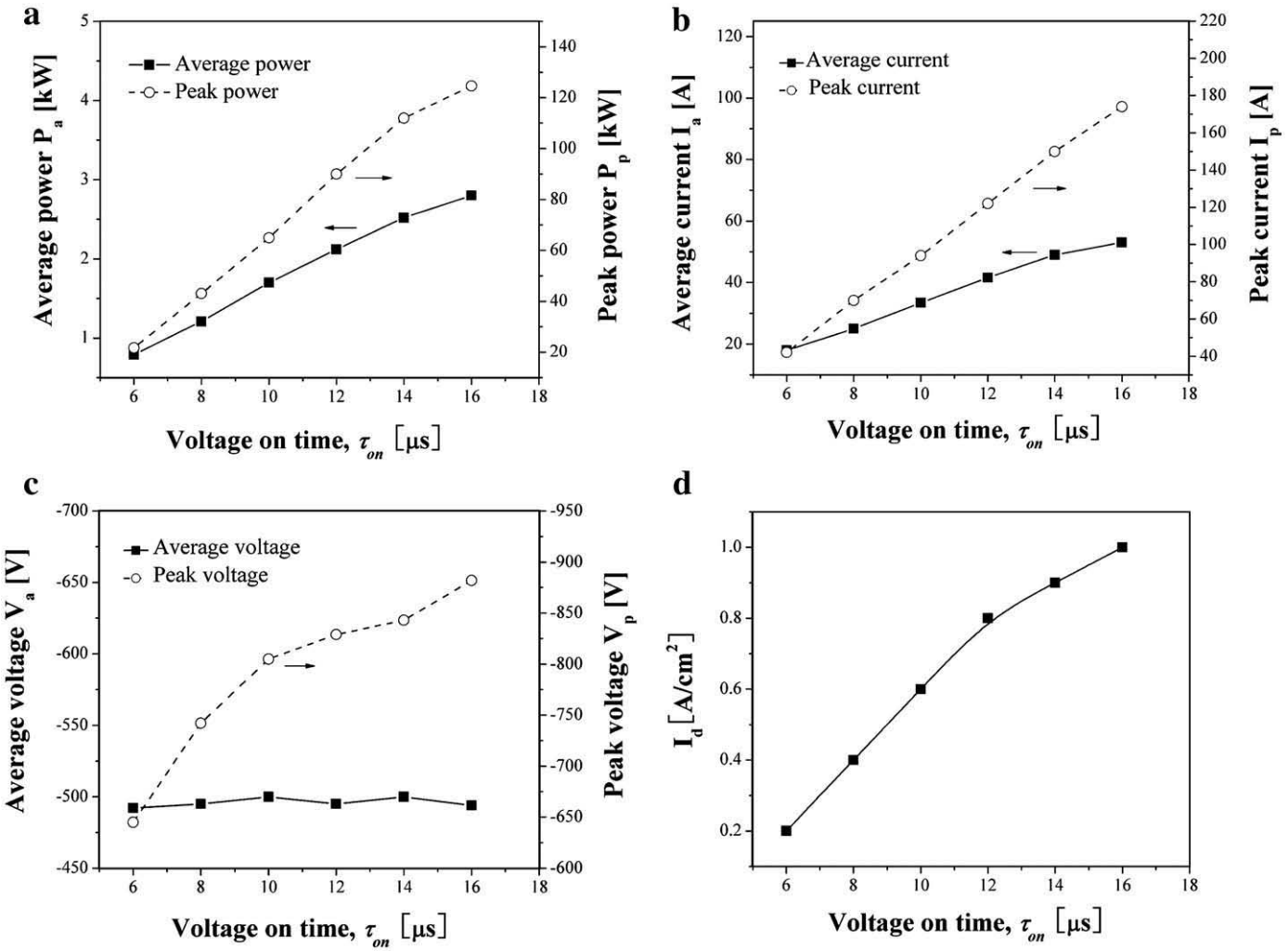

Fig. 3. The variations of (a) the target power, (b) current, (c) voltage and (d) target current density developed on the Cr target as a function of τ_{on} for MPP sputtering.

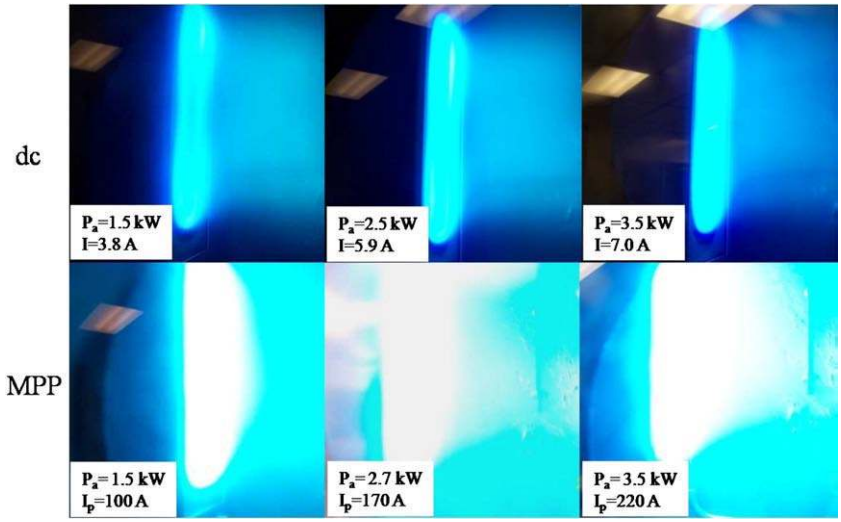

Fig. 4. Photos showing the comparison of the light emission intensities between dc and MPP plasma at different average target powers and peak currents.

maximum signal intensity. The same tuning parameters were applied for all plasma measurements in an effort to keep a consistent comparison for the results. A negative voltage of −25 V was applied on the low energy extractor in the EQP to assist the extract of the ions from the plasma. The IED scans were measured from −5 to 100 V with a step size of 0.5 V and 100 ms dwell time. The IMDs were scanned from 0.4 to 100 m/e with 0.2 step size and 100 ms dwell time at an ion energy of 5 eV. An oscilloscope was integrated in the MPP generator's control module to give its capability of monitoring the real time output voltage, current and power waveforms on the target.

3. Results and discussion

3.1. MPP and dc discharge plasma

As introduced in the previous section, by controlling the pulse width, the frequency, and τ_{on} and τ_{off} in the micro pulses (Fig. 1), MPP can generate various powers and currents on the target. Fig. 3 shows the variation of the target power, current, voltage, and current density developed on the Cr target as the τ_{on} in the strongly ionized period was increased from 6 to 16 μs, while maintaining other pulse parameters constant as explained in the Experimental section.

The peak and average power (P_p and P_a) and the peak and average current (I_p and I_a) on the Cr target increased almost linearly with an increase in the τ_{on} from 6 to 14 μs, but then the rate slightly decreased as the τ_{on} was increased from 14 to 16 μs. when the τ_{on} is at 16 μs, the P_p and I_p on the target reach 125 kW and 175 A respectively. The average voltage (V_a) on the target exhibited a small variation from −492 to −500 V. However, the peak voltage (V_p) increased from −645 to − 882 V as the τ_{on} was increased. Using the effective sputtering area of 180 mm^2, the peak current density (I_d) on the target can thereby be obtained and is plotted in Fig. 3d, which shows that the I_d increased from 0.2 to 1.0 A/cm^2 when the τ_{on} was increased from 6 to 16 μs. These MPP pulse conditions were used for the plasma diagnostics in the present study.

Fig. 4 presents photos showing the light emission intensities of dc and MPP plasma at similar average target powers during Cr sputtering in pure Ar. The intensity of the light emission is controlled by the number density of excited atoms in the plasma, which in turn is a reflection of the plasma density. Variation in the intensity of the light emission can therefore be considered as an indication of changes in the plasma density. The dc discharges generated from 1.5 to 3.5 kW target powers exhibit low light emission intensities which are visualized in blue color. Based on the visualization, the brightest sheath in the plasma, where most excitation collisions took place, exhibits low intensity and slightly extends away from the target surface as the target power was increased. In addition, it is clear that the plasma region is mainly confined in front of the target. On the other hand, the MPP plasma generated at similar average target powers, but with much higher peak currents and powers, exhibits extremely high light emission intensities (bright white color), indicating significant increased number densities of the excited

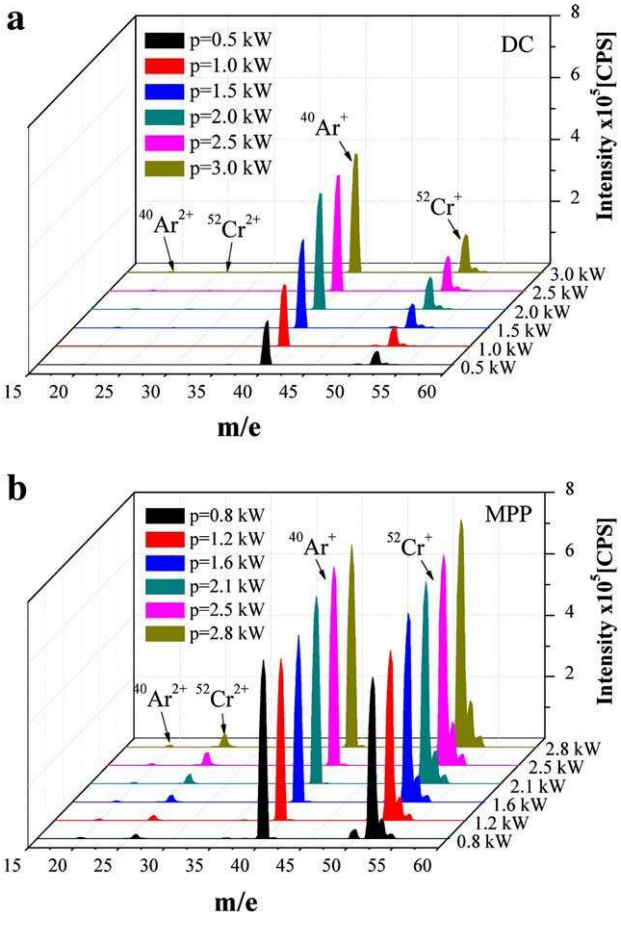

Fig. 5. Ion mass distributions of (a) dc plasma and (b) MPP plasma, generated at different average target powers during sputtering a Cr target in pure Ar atmosphere.

atoms in the plasma. It also can be seen that the brightest part within the plasma extends far away from the target surface as the peak power and current were increased. Additionally, the plasma region is not only confined in front of the target but extends to the whole of the chamber. This comparison indeed demonstrates the great advantage of the MPP/HPPMS technique in utilizing pulsed high peak power and current on the target to achieve high plasma densities and ionization degrees but avoiding high thermal load on the target with comparable average target powers to the continuous dc technique.

3.2. Ion mass distributions of MPP and dc plasma

Fig. 5 shows the comparison of the positive IMDs measured using the EQP for dc and MPP discharges generated by sputtering the Cr target in pure Ar at different P_a (the I_p, V_p, and P_p in MPP can be seen in Fig. 3). As shown in Fig. 5a, the dc plasma contains the ion species of $^{52}Cr^+$, $^{40}Ar^+$, and their isotopes, and a very small number of $^{52}Cr^{2+}$ and $^{40}Ar^{2+}$ double charged ions at high powers. The intensities of the $^{40}Ar^+$ ions obtained at all dc powers are much higher than the metal $^{52}Cr^+$ ions, suggesting that the major ions in the dc discharge plasma are from the sputtering gas species while the degree of ionization of the metal target atoms is very low. The numbers of $^{40}Ar^+$ and $^{52}Cr^+$ ions increase with an increase in the dc target power from 0.5 to 3.0 kW.

On the other hand, the MPP plasma obtained at similar P_a exhibits considerable increases in the peak intensities for all ion species ($^{40}Ar^+$, $^{52}Cr^+$, $^{52}Cr^{2+}$ and $^{40}Ar^{2+}$), especially for the metal ion species ($^{52}Cr^+$ and $^{52}Cr^{2+}$) as compared to the dc plasma (Fig. 5b). The intensities of all ion species steadily increased as the P_a was increased. It can be seen that the $^{40}Ar^+$ peak intensity is slightly higher than the $^{52}Cr^+$ peak at $\tau_{on}=\tau_{off}=6$ μs ($P_a=0.8$ kW, $P_p=22$ kW, $I_p=42$ A) condition. With further increases of the τ_{on} from 8 to 16 μs, which correspond to an increase in the P_a from 1.2 to 2.8 kW, P_p from 43 to 125 kW, and I_p from 70 to 175 A (see Fig. 3), the intensities of the metal $^{52}Cr^+$ peaks are higher than the $^{40}Ar^+$ peaks, which suggests a significant increase in the metal ion species in the plasma as the target power and current were increased in the MPP conditions.

To examine the IMD in more detail, the mass distributions obtained for dc conditions at target powers of 1.0 and 2.5 kW and for MPP conditions at P_a of 1.2 and 2.5 kW were plotted in log10 scale and presented in Fig. 6. It can be seen that all scans contain small numbers of $^1H^+$ and $^{32}O_2^+$ which are from the residual water vapor and O_2 in the vacuum system. The dc plasma at 1.0 kW target power shows $^{52}Cr^+$ peak and its isotopes, $^{40}Ar^+$ peak and its isotopes, a few double ionized $^{40}Ar^{2+}$, and very small number of double ionized $^{52}Cr^{2+}$ (Fig. 6a). As the target power was increased to 2.5 kW, as shown in Fig. 6b, the peak intensities for all ion species increased, and possible $^{52}Cr^{3+}$ ($m/e=17.3$) and $^{52}Cr^{4+}$ ($m/e=13$) peaks were revealed. In contrast, an intense $^{52}Cr^{2+}$ peak and its isotopes and possible small numbers of $^{52}Cr^{3+}$ and $^{52}Cr^{4+}$ were identified in the MPP discharge even at a low P_a of 1.2 kW ($P_p=43$ kW, $I_p=70$ A) (Fig. 6c). Further increasing the P_a to 2.5 kW ($P_p=112$ kW, $I_p=150$ A) led to further increased intensities in all metal ion species (Fig. 6d). However, it should be noted that the peaks at around $m/e=13$ for $^{52}Cr^{4+}$ and $m/e=17.3$ for $^{52}Cr^{3+}$ are not well resolved from a possible N^+ peak at $m/e=14$ and a possible H_2O^+ peak at $m/e=18$ and require more work to confirm.

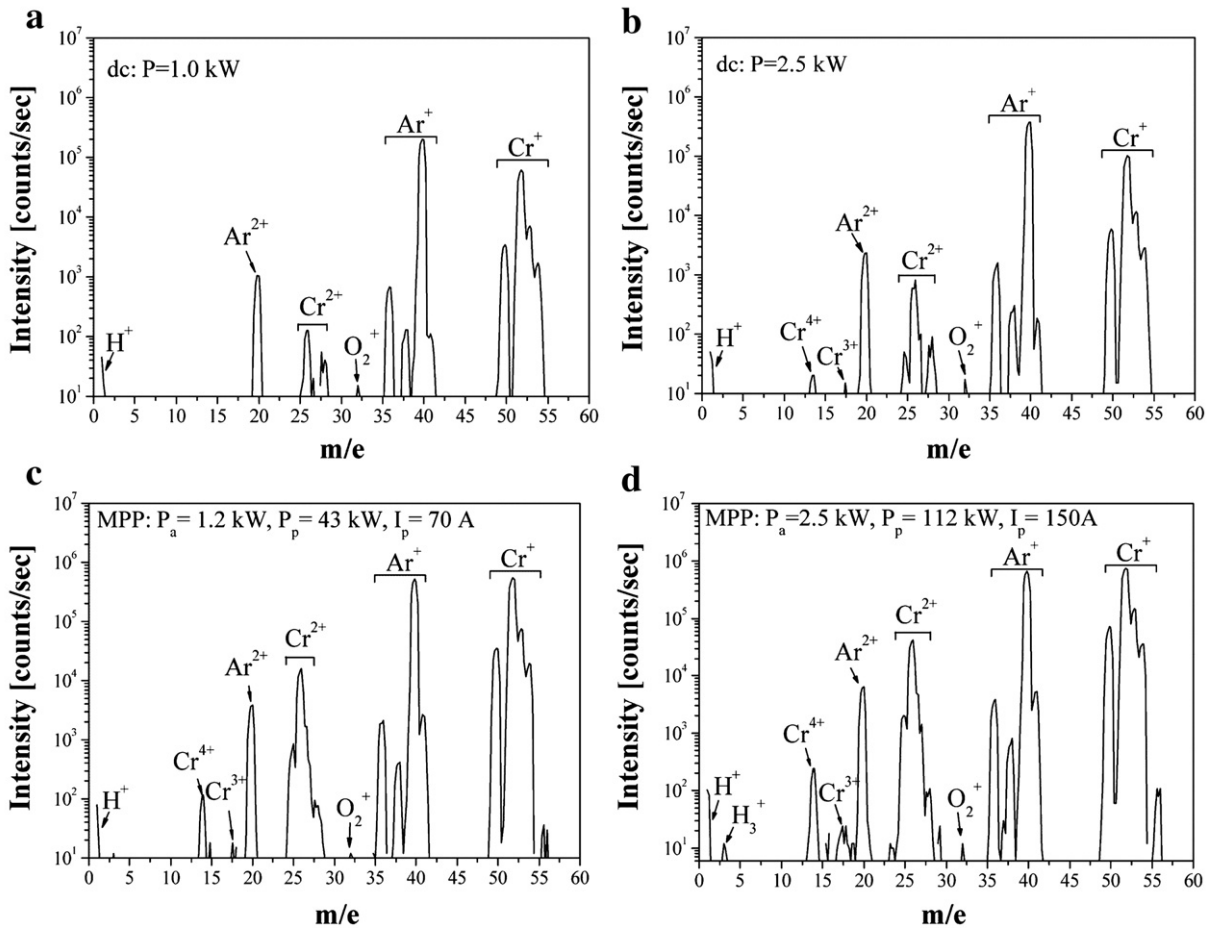

Fig. 6. Ion mass distributions (plotted in log10 scale) of dc plasma at target powers of (a) 1.0 kW, (b) 2.5 kW, and MPP plasma at average target powers of (c) 1.2 kW, (d) 2.5 kW, during sputtering a Cr target in pure Ar atmosphere.

3.3. IEDs of MPP plasma in pure Ar atmosphere

A comparison of the time averaged IEDs for $^{40}Ar^+$, $^{52}Cr^+$ and $^{52}Cr^{2+}$ ion species measured from the MPP plasma obtained at different τ_{on} times (6, 8, and 16 μs) during Cr sputtering is presented in Fig. 7. The IED of the continuous dc plasma with a target power of 2 kW is also plotted in Fig. 7 for comparison. The I_p, V_p, and P_a values on the cathode in the MPP conditions are also given in Fig. 7. It can be seen that a small number of ions shows with 'negative energy' values in the IED curves. These ions have not been sampled from the plasma but have in fact been created inside the EQP between the sampling orifice (grounded) and the extractor (negative) by electrons entering into that region. Small numbers of such ions will be seen at these 'negative energies' possibly as far as the negative voltage applied to the extractor, and should be discounted.

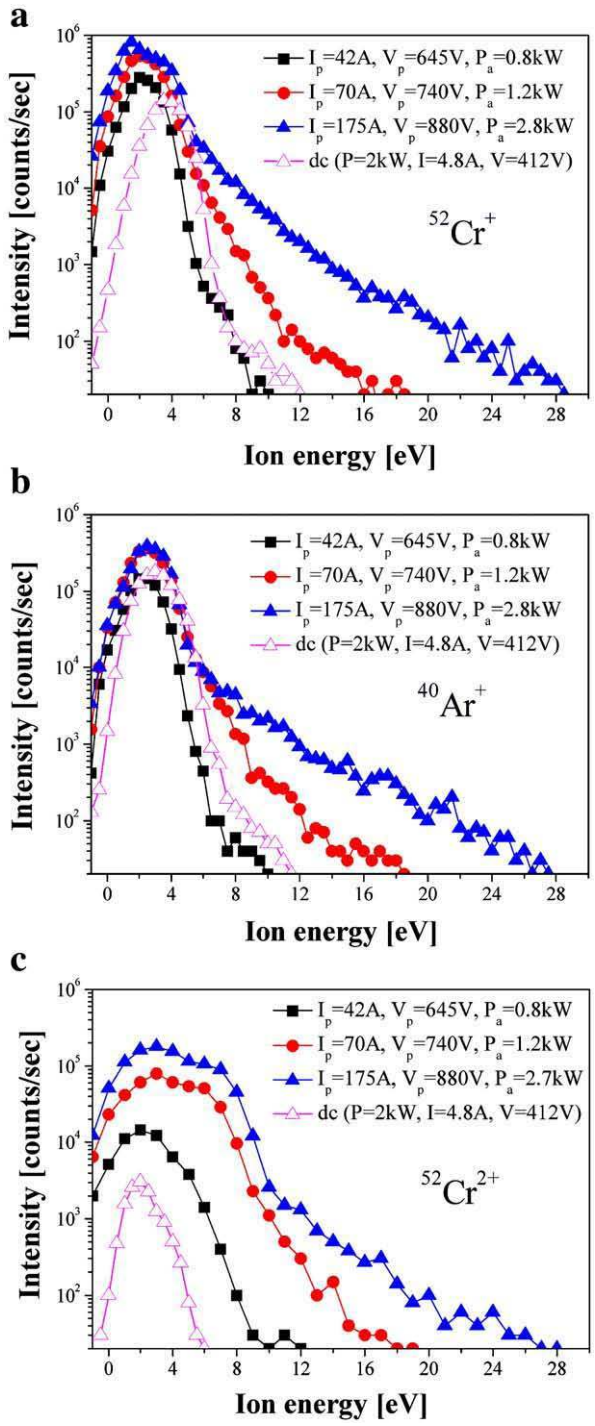

Fig. 7. A comparison of the ion energy distributions of (a) $^{52}Cr^+$, (b) $^{40}Ar^+$, and (c) $^{52}Cr^{2+}$ species measured from MPP plasma with different peak currents and dc plasma with average target power of 2 kW during sputtering a Cr target in pure Ar atmosphere.

A low ion energy peak and a short energy tail can be identified in both dc and MPP IEDs for $^{40}Ar^+$, $^{52}Cr^+$ and $^{52}Cr^{2+}$ ions. The continuous dc IED exhibits a peak energy of about 4–5 eV, and the maximum energy for the energy tail is about 12 eV. The significant intensity of $^{52}Cr^+$ ions observed in the dc plasma is possibly due to the closed magnetic field configuration of the current deposition system, which can effectively reduce the loss of electrons to the chamber wall and thereby increasing the ion and plasma density. The MPP IEDs exhibit a lower peak energy of about 1–2 eV. An increase in the peak current and power of the MPP led to a slight change of the low energy peak position toward lower ion energy values for $^{52}Cr^+$ ions and toward higher ion energy values for $^{40}Ar^+$ and $^{52}Cr^{2+}$ ions. However, the maximum ion energies in the tail for all ion species extend toward higher energies as the I_p, V_p and P_a were increased. In general, the peak ion energy comes from the energy gained by the ion species in crossing the sheath from the plasma to the grounded EQP probe, therefore it represents the plasma potential, which is about 4–5 eV in the dc condition and 1–2 eV in the MPP condition as observed in the present work (Fig. 7). For the $^{52}Cr^+$ ions, the ion energies in the tail originate in the distribution of the kinetic energies of the ejected target (Cr) neutral atoms, which is strongly determined by the kinetic energy of the Ar^+ ions bombarding the target, the binding energy of the target material, and sputter yield as described by Thompson's Theory [41]. Consequently, an increase in the V_p on the Cr target will increase the kinetic energy of incoming Ar^+ ions, which is then transferred to the ejected Cr neutral atoms, thereby extending the maximum ion energies of the IED tails. Nevertheless, it should be noted that the intensity ($<10^3$ c/s in log10 scale) and the energy range (<30 eV) of the energy tails in all MPP plasmas studied in the present work are low and the main contribution to the total ion energy transported to the sampling orifice of the analyzer (or substrate during deposition) comes from the low energy peak region (1–2 eV).

The $^{40}Ar^+$ IEDs exhibit similar maximum ion energies to those shown by the $^{52}Cr^+$ ions for both dc and MPP IEDs (Fig. 7b). The Cr atoms are ejected from the cathode with high energies and lose some of the energy in thermalising collisions with the background gas atoms. Consequently, the $^{40}Ar^+$ ions in the main low energy peak correspond to thermalized species ionized at plasma potential, whereas the energies in the high energy tail are gained from the collisions with either the $^{52}Cr^+$ ions or sputtered Cr neutral atoms. Hecimovic et al. showed that the ion energy tail of gas ions in HIPIMS discharges have different shapes for different pressures. At a low pressure, the tail of gas ions exhibited two Maxwellian distributions similar to the ones found for metal ions whereas the gas ions comprised only a single low energy peak at high pressure [11]. Similar influence of the pressure on the gas ion energy distributions was also observed in the dc plasma [42]. Bases on Hecimovic's observations, it may be speculated that the similar maximum energies in the ion energy tails for the $^{40}Ar^+$ and $^{52}Cr^+$ ions in the current study is probably because of the low working pressure (0.67 Pa). It would be interesting to compare the IED of the gas ions in the MPP plasma under higher working pressures in the future studies.

The IEDs of $^{52}Cr^{2+}$ plotted in Fig. 7c, exhibit slightly higher peak ion energies than the $^{40}Ar^+$ and $^{52}Cr^+$ species. The maximum ion energies measured from the ion energy tail are about 12 eV for the dc discharge and 10 to 28 eV for the MPP discharges. These values have been obtained from the raw experimental data by multiplying with the charge state (2+) on the assumption that they refer to doubly-charged ions of mass 52 rather than to single charged unknown ions of mass 26. The ion energies are consistent with the view that the main part of

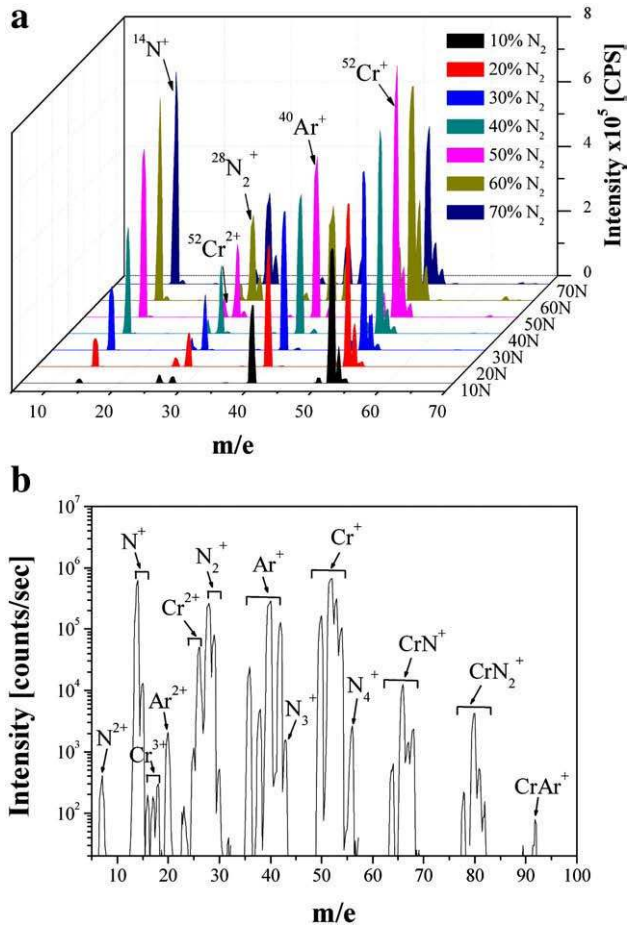

Fig. 8. (a) Ion mass distributions of MPP sputtering of Cr in a Ar/N_2 mixture versus different N_2 percentages and (b) Ion mass distribution of MPP sputtering of Cr at 50% N_2 (plotted in log10 scale).

the energy has been inherited from the parent chromium atoms ejected from the cathode, with the addition of about 2 to 4 eV (in the case of the MPP discharges) from the plasma potential.

Similar to the observations in the IMD scans, the IED scans confirm that much higher numbers of target/metal ion species ($^{52}Cr^+$ and $^{52}Cr^{2+}$) were obtained in the MPP plasma as compared to the dc plasma, in which the integrated areas under the $^{52}Cr^+$ and $^{52}Cr^{2+}$ curves (relevant to the ion flux) in MPP ($P_a = 1.2$ kW) are about 5 and 33 times higher than those in dc discharge of higher powered ($P = 2$ kW), respectively.

It should be emphasized that other IED measurements were carried out by installing the EQP probe facing the Cr target at a distance to the target surface approximately of 145 mm and removing the other cathode out of the deposition system. In this condition, the magnetic field in the deposition system is not closed. It was found that the ions ($^{52}Cr^+$, $^{52}Cr^{2+}$ and $^{40}Ar^+$) exhibited similar IEDs to those measured when the EQP was installed parallel to the target surface. These IED curves also show a peak ion energies at 1–2 eV and a short ion energy tail with the maximum ion energy determined by the peak voltage and current on the cathode. However, different intensities of the ions in the IED curves were observed.

3.4. IMDs and IEDs of the MPP plasma in an Ar/N_2 atmosphere

To investigate the MPP plasma properties in the reactive sputtering condition, the N_2 flow rate percentage (f_{N2}) was varied from 10% to 100% in the deposition system. The MPP pulse parameters are: the total pulse width was 750 μs, the pulse frequency was 100 Hz, and the τ_{off} and τ_{on} within the micro pulse were 6 and 10 μs, respectively. This pulse condition generated P_a and P_p values of 1.6 kW and 65 kW, I_a and I_p of 33 and 94 A, and V_a and V_p of − 500 and − 820 V, respectively on the cathode at the 0% N_2 condition (see Fig. 3).

The IMDs measured for the MPP plasma for sputtering Cr target in an Ar/N_2 atmosphere for different f_{N2} percentages are presented in Fig. 8a. The intensities of both $^{14}N^+$ and $^{28}N_2^+$ species increased as the f_{N2} was increased from 10% to 70% in the chamber. Furthermore, the intensities of $^{14}N^+$ ions are much higher than the $^{28}N_2^+$ species when the f_{N2} is above 20%. The $^{52}Cr^+$, $^{52}Cr^{2+}$ and $^{40}Ar^+$ species increased in intensity as the f_{N2} was increased from 10% to 50%, but then they decreased with further increases of f_{N2} in the system. These variations can be explained by the target 'poisoning' effect when the f_{N2} was above 50% in the system. In this case, the formation of the nitride compound layer on the target surface, which usually exhibits a much

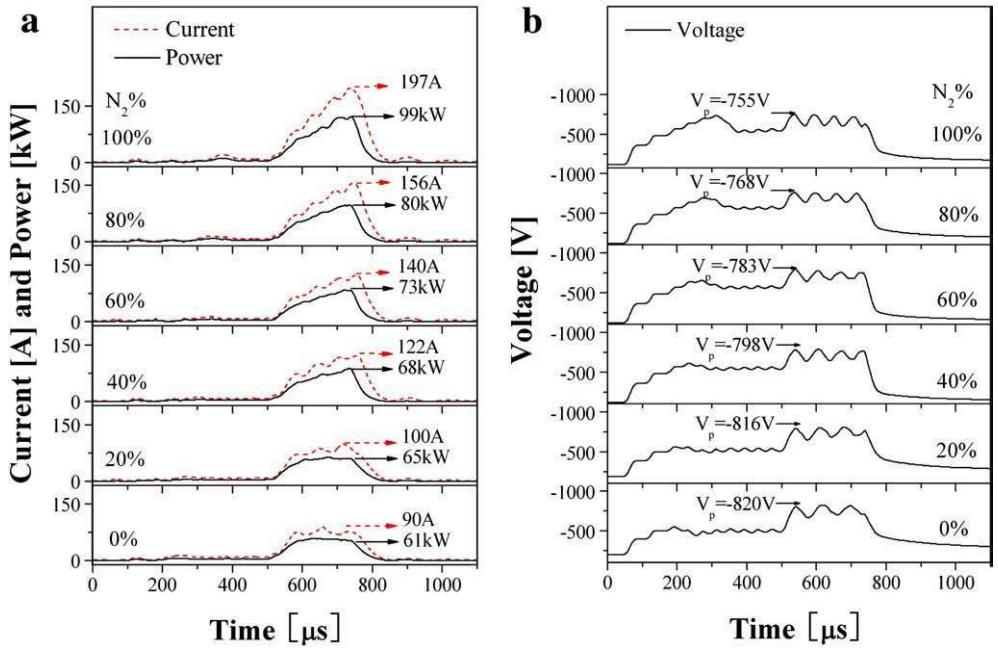

Fig. 9. (a) The current and power, and (b) voltage waveforms developed on the Cr target at different f_{N2} percentages in the system (the peak values are labeled in the figures).

lower sputtering yield than that of the pure metal target, leads to a drop in the number of sputtered Cr atoms, which results in the decrease in the formation of the Cr and Ar ions. However, it should be noted that the reduction of the number of $^{52}Cr^{+}$ ions is small, and they still exhibit significant high intensity at high f_{N2}. The high degree of ionization of the target material in the reactive sputtering conditions possibly improves the hysteresis effect resistance in the MPP technique. Recently, Wallin and Helmersson [43] have observed a reduced or eliminated hysteresis effect by using HIPIMS during the reactive sputtering of an Al target in Ar/O_2 atmosphere. They attributed this improvement to the increased effective target current density in HIPIMS process, which accounts for the creation of a high flux of the target material during the pulse and a possible rarefaction of reactive gas in front of the target.

The IMD obtained at 50% N_2 is plotted in log10 scale and is shown in Fig. 8b as a typical example to further identify ion species presented in the MPP plasma. It can be seen that single, double, and triple ionized metal and gas species are identified in the MPP plasma. For the metal ion species, the single charged Cr^{+} ions with isotope peaks at $m/e = 50$–54, the double charged Cr^{2+} ions at

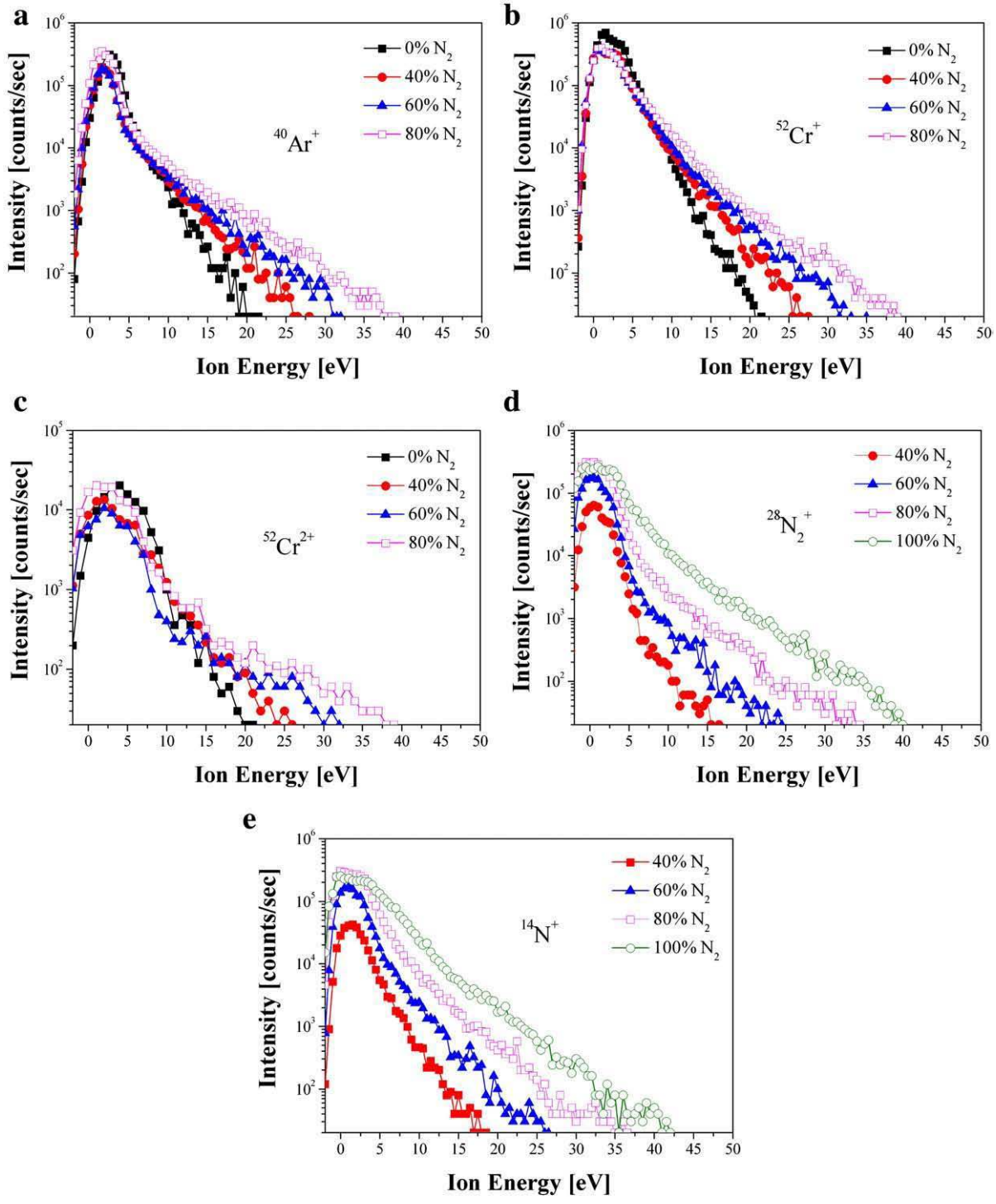

Fig. 10. Ion energy distributions of (a) $^{40}Ar^{+}$, (b) $^{52}Cr^{+}$, (c) $^{52}Cr^{2+}$, (d) $^{28}N_2^{+}$ and (e) $^{14}N^{+}$ ions measured from the MPP plasma during sputtering a Cr target in a Ar/N_2 mixture with different N_2 percentages in the system.

$m/e = 25–26$, and the triple charged Cr^{3+} ions at $m/e = 16–18$ were identified. The gas ion species include $Ar^+(m/e = 36–41)$, $Ar^{2+}(m/e = 20)$, $N^+(m/e = 14–15)$, $N^{2+}(m/e = 7)$, $N_2^+(m/e = 28–29)$, $N_3^+(m/e = 42)$ and $N_4^+(m/e = 56)$. In addition, ion species of CrN^+ with isotope peaks ($m/e = 64–68$), CrN_2^+ with isotope peaks ($m/e = 78–82$) were also observed. The weak peak at $m/e = 92$ is possibly from the $(CrAr)^+$ but need further investigation to confirm.

The current, power, and voltage waveforms developed on the Cr target for one MPP pulse width at different f_{N2} percentages are presented in Fig. 9a and b respectively. The I_p, P_p and V_p values were labeled in the figures. When the f_{N2} was increased in the system, the waveforms of the discharge current and power during the strongly ionized pulse period were gradually changed from level to tilted shapes. The maximum I_p increased from 90 to 197 A, and P_p increased from 61 to 99 kW when the f_{N2} was increased from 0% to 100%. It was also found that the measured V_a exhibits a small variation between −540 and −550 V (not shown here). However, V_p on the target decreased from −840 to −776 V when f_{N2} was increased from 0% to 100% in the system.

The variation of the target I_p and V_p at different f_{N2} percentages can be explained by the target 'poisoning' effect. In the reactive sputtering condition, the N_2 will react with the Cr target to form nitride compounds on the target surface. The formation of the nitride compound on the Cr target surface leads to an increase in the target current since the nitride compounds exhibit higher ion-induced secondary electron emission yields (ISEE) compared to a metallic Cr target [44]. When the f_{N2} is low (<40%), as shown in Fig. 9a, there was a slight increase in the target peak current, suggesting that the 'poisoning' effect on the target is low. Further increase in the f_{N2} from 40% to 100% led to pronounced and steep increases in the target peak current and power, indicating the rapid formation of a nitride compound layer on the target surface. The reversed trend of a decrease in the cathode voltage is also the consequence of the increased ISEE on the target surface as the coverage of the nitride compounds increased at higher f_{N2}.

The increased I_p and P_p on the Cr target as the f_{N2} was increased will affect the positive IEDs of the ion species in the MPP plasma. Fig. 10 shows the positive IEDs of $^{40}Ar^+$, $^{52}Cr^+$, $^{52}Cr^{2+}$, $^{28}N_2^+$, and $^{14}N^+$ species measured at different f_{N2} percentages. The increase in the N_2 flow led to a slight change of the low energy peak position toward a lower ion energy value for all ion species. Nevertheless, it is evident that the maximum ion energy of the energy tail extended to higher energies for all ion species as the f_{N2} was increased in the system. This phenomenon is related to the increased I_p and P_p on the Cr target as shown in Fig. 9a. Similar to the observations in the pure Ar atmosphere condition (non-reactive sputtering) as show in Fig. 7, it can be seen that the maximum ion energy of $^{40}Ar^+$ is about the same as the $^{52}Cr^+$ for all Ar/N_2 reactive sputtering conditions (Fig. 10a and b), suggesting that the $^{40}Ar^+$ ions still gain their energies from collisions with the energetic Cr neutral atoms ejected from the target or from collisions with energetic Cr^+ ions whose ion energy are set by the neutral distribution. The energy of double ionized $^{52}Cr^{2+}$ ions are again plotted by multiplying the raw experimental data with the charge state (2+). It shows that the true energy distributions of double ionized $^{52}Cr^{2+}$ ions and the single ionized $^{52}Cr^+$ ions are the same (Fig. 10c), apart from a small difference due to the energy acquired in crossing the sheath in front of the EQP orifice.

As for the $^{28}N_2^+$ and $^{14}N^+$ ion species, they exhibit smaller maximum ion energies of the tail as compared to those of the $^{40}Ar^+$ and $^{52}Cr^+$ ions (Fig. 10d and e). It is expected that additional collision and ionization processes including possible charge exchange collisions with Ar^+ or Penning ionization which will affect the energies of the nitrogen ions. However, the difference in the maximum ion energies between the N ions and the Ar and Cr ions became smaller at higher f_{N2}.

4. Conclusions

The ion energy and mass distributions of the positive ions in the plasma during MPP magnetron sputtering of a Cr target in pure Ar and Ar/N_2 atmospheres were investigated and compared with the plasma properties obtained using continuous dc magnetron sputtering with similar average target powers.

In the pure Ar atmosphere, single and double ionized Cr and Ar ion species were identified in the MPP plasma. Significant increases in the number of both target material (Cr) and gas (Ar) ions for a MPP plasma compared to a continuous dc plasma were demonstrated. The number of ions increased as the average target power (as well as the peak power and peak current) was increased during the MPP sputtering. Examination of the ion energy distributions shows that the MPP discharge provides an almost mono-energetic source of ions with a peak ion energies at 1–2 eV and a short ion energy tail (<30 eV) with the maximum ion energy affected by the peak voltage and current on the cathode.

In the Ar/N_2 mixture, a wide variety of ion species including single, double, triple ionized Cr, Ar and N ions, N_3^+, N_4^+, CrN^+, CrN_2^+ and $CrAr^+$ ions were identified in the MPP discharge. It was found that the peak current and power on the Cr target increased significantly, while the peak voltage decreased as the N_2 flow rate percentage was increased in the chamber. The ion energy distributions of ion species of MPP plasma in Ar/N_2 atmosphere exhibited similar peak values and tail distributions as compared to the MPP plasma measured in a pure Ar atmosphere. However, an increase in the maximum ion energy of the energy tail with the increasing of the N_2 flow rate percentage was observed due to the increased target peak current and power from the 'target poisoning' effect.

Acknowledgement

We acknowledge the support of the MPP generator for the research program from the Zpulser, LLC, USA.

References

[1] V. Kouznetsov, K. Macák, J.M. Schneider, U. Helmersson, I. Petrov, Surf. Coat. Technol. 122 (1999) 290.
[2] W.D. Sproul, D.J. Christie, D.C. Carter, Proceedings of the 47th Annual SVC Technical Conference, Dallas, Texas, April 25–29, 2004, pp. 96–100.
[3] K. Macak, V. Kouznetsov, J.M. Schneider, U. Helmersson, I. Petrov, J. Vac. Sci. Technol. A 18 (2000) 1533.
[4] D.J. Christie, F. Tomasel, W.D. Sproul, D.C. Carter, J. Vac. Sci. Technol. A 22 (4) (2004) 1415.
[5] C. Christou, Z.H. Barber, J. Vac. Sci. Technol. A 18 (2000) 2897.
[6] A.P. Ehiasarian, R. New, W.-D. Munz, L. Hultman, U. Helmersson, V. Kouznetsov, Vacuum 65 (2002) 147.
[7] J. Bohlmark, M. Lattemann, J.T. Gudmundsson, A.P. Ehiasarian, Y. Aranda Gonzalvo, N. Brenning, U. Helmersson, Thin Solid Films 515 (2006) 1522.
[8] K. Burcalova, A. Hecimovie, A.P. Ehiasarian, J. Phys. D: Appl. Phys. 41 (2008) 115306.
[9] S. Konstantinidisa, J.P. Dauchot, M. Ganciu, A. Ricard, M. Hecq, J. Appl. Phys. 99 (2006) 013307.
[10] D. Horwat, A. Anders, J. Phys. D: Appl. Phys. 41 (2008) 135210.
[11] A. Hecimovic, K. Burcalova, A.P. Ehiasarian, J. Phys. D: Appl. Phys. 41 (2008) 095203.
[12] A. Vetushka, A.P. Ehiasarian, J. Phys. D: Appl. Phys. 41 (2008) 015204.
[13] N. Brenning, I. Axnas, M.A. Raadu, D. Lundin, U. Helmerson, Plasma Sources Sci. Technol. 17 (2008) 045009.
[14] A.P. Ehiasarian, A. Vetushka, A. Hecimovic, S. Konstantinidis, J. Appl. Phys. 104 (2008) 083305.
[15] K.B. Gylfason, J. Alami, U. Helmersson, J.T. Gudmundsson, J. Phys. D: Appl. Phys. 38 (2005) 3417.
[16] A. Anders, J. Andersson, A. Ehiasarian, J. Appl. Phys. 102 (2007) 113303.
[17] Jaroslav Vlček, Pavel Kudláček, Kristýna Burcalová, Jindřich Musil, J. Vac. Sci. Technol. A 25 (1) (2007) 42.
[18] Ulf Helmersson, Martina Lattemann, Johan Bohlmark, Arutiun P. Ehiasarian, Jon Tomas Gudmundsson, Thin Solid Films 513 (2006) 1–24.
[19] A.P. Ehiasarian, P.Eh. Horsepian, L. Hultman, U. Helmersson, Thin Solid Films 457 (2004) 270.
[20] J. Alami, K. Sarakinos, F. Uslu, M. Wuttig, J. Phys. D: Appl. Phys. 42 (2009) 015304.
[21] K. Sarakinos, J. Wördenweber, F. Uslu, P. Schulz, J. Alami, M. Wuttig, Surf. Coat. Technol. 202 (2008) 2323.
[22] S. Konstantinidis, J.P. Dauchot, M. Hecq, Thin Solid Films 515 (2006) 1182.
[23] K. Sarakinos, J. Alami, C. Klever, M. Wuttig, Surf. Coat. Technol. 202 (2008) 5033.

[24] V. Sittinger, F. Ruske, W. Werner, C. Jacobs, B. Szyszka, D.J. Christie, Thin Solid Films 516 (2008) 5847.
[25] C. Reinhard, A.P. Ehiasarian, P.Eh. Hovsepian, Thin Solid Films 515 (2007) 3685.
[26] J. Alami, P.O.Å. Persson, D. Music, J.T. Gudmundsson, J. Bohlmark, U. Helmersson, J. Vac. Sci. Technol. A 23 (2) (2005) 278–280.
[27] K. Bobzin, N. Bagcivan, P. Immich, S. Bolz, R. Cremer, T. Leyendecker, Thin Solid Films 517 (2008) 1251–1256.
[28] K. Yukimura, R. Mieda, H. Tamagaki, T. Okimoto, Surf. Coat. Technol. 202 (2008) 5246.
[29] M. Lattemann, A.P. Ehiasarian, J. Bohlmark, P.Å.O. Persson, U. Helmersson, Surf. Coat. Technol. 200 (2006) 6495.
[30] A. Anders, Phys. Status Solidi (A) 205 (4) (2008) 965.
[31] A.P. Ehiasarian, J.G. Wen, I. Petrov, J. Appl. Phys. 101 (2007) 054301.
[32] W.D. Sproul, D.J. Christie, D.C. Carter, Proceedings of the 47th Annual SVC Technical Conference, Dallas, Texas, April 25–29, 2004, pp. 96–100.
[33] D.J. Christie, J. Vac. Sci. Technol. A 23 (2) (2005) 330.
[34] Roman Chistyakov, Bassam Abraham, William D. Sproul, Proceedings of the 49th Annual SVC Technical Conference, Washington, DC, April 23–27, 2006, pp. 16–19.
[35] R. Chistyakov, B. Abraham, W. Sproul, J. Moore, J. Lin, Proceedings of the 50th Annual SVC Technical Conference, Louisville, KY, April 30–May 3, 2007, pp. 139–143.
[36] William D. Sproul, Roman Chistyakov, Bassam Abraham, Society of Vacuum Coaters News Bulletin, Summer 2006, pp. 35–37.
[37] R. Chistyakov, U.S. Patent 6,896,773, "High Deposition Rate Sputtering," May 24, 2005.
[38] R. Chistyakov, U.S. Patent 7,147,759, "High-Power Pulsed Magnetron Sputtering," December 12, 2006.
[39] R. Chistyakov, U.S. 7,095,179, "Methods and apparatus for generating strongly-ionized plasmas with ionizational instabilities," August 22, 2006.
[40] R. Chistyakov, U.S. 7,345,429, "Methods and apparatus for generating strongly-ionized plasmas with ionizational instabilities," March 18, 2008.
[41] M.W. Thompson, Philos. Mag. 18 (1968) 377.
[42] S. Kadlec, C. Quaeyhaegens, G. Knuyt, L.M. Stals, Surf. Coat. Technol. 89 (1997) 177–184.
[43] E. Wallin, U. Helmersson, Thin Solid Films 516 (2008) 6398.
[44] Zenghu Han, Jiawan Tian, Qianxi Lai, Xiaojiang Yu, Geyang Li, Surf. Coat. Technol. 162 (2003) 189–193.